npj | flexible electronics

www.nature.com/npjflexelectron

ARTICLE OPEN

Check for updates

Large-scale fully printed "Lego Bricks" type wearable sweat sensor for physical activity monitoring

Wenhui Ji[1,4], Huanzhuan Liu[1,4], Yadong Liu[1], Wei Zhang[1], Tong Zhou[1], Xinxin Liu[1], Chao Tao[2], Jiangxuan Dai[3], Baoli Zha[1], Ruijie Xie[3], Jiansheng Wu[1], Qiong Wu[1]✉, Weina Zhang[1], Lin Li[1,3]✉ and Fengwei Huo[1,3]✉

Wearable sweat sensors are becoming increasingly popular for their robust capabilities in non-invasive, dynamic, and continuous real-time monitoring of biological information. Real-time monitoring of large-scale samples is crucial for realizing intelligent health. A major bottleneck for enabling large-scale sweat elucidation is the fabrication of wearable sensors equipped with microfluidic devices and flexible electrodes in a cost-effective, homogeneous performance and rapid large-scale way. Herein, a "Screen+Wax"-printing technique was introduced to prepare these components and construct "Lego Bricks" type wearable sweat sensor sensor to monitor sweat Na^+ and K^+. Flexible electrode arrays and paper-based microfluidic layers (they act as building blocks) were fabricated on polyethylene terephthalate and paper surfaces, respectively, using screen printing and wax printing. Gold nanoparticles and Na^+/K^+ ion-selective membranes were modified on the electrode surfaces by electrodeposition and drop coating, respectively. In this work, we highlight the excellent performance of the "Lego Bricks" type wearable sweat sensor in testing the Na^+ and K^+ imbalance of sweat from different body regions during exercise and, more significantly, to track the physical activity during prolonged exercise under different interventions. Furthermore, the prepared "Lego Bricks" wearable sweat ion electrochemical sensor is demonstrated to be capable of large-scale samples elucidation with outstanding performance and cost-effectiveness, which is expected to deeply integrate sweat monitoring into physical activity, providing an important tool for intelligent health.

npj Flexible Electronics (2023)7:53 ; https://doi.org/10.1038/s41528-023-00285-w

INTRODUCTION

Global warming has been worsening in recent years, which poses a significant threat to individuals who work or engage in physical activities in hot environments as they are at high risk of thermal-related diseases (Fig. 1a). To prevent and diagnose these diseases, traditional methods usually rely on analyzing variations of biomarkers in multiple biological fluids such as blood and saliva[1,2]. However, these methods have several drawbacks such as invasive/minimally invasive detection, high cost, time-consuming analysis, and susceptibility to sample contamination, which limit their widespread application[3–5]. Numerous studies have shown that human sweat contains a wealth of biochemical information that can reflect the hydration status of the body and indicators of thermal-related diseases through non-invasive monitoring[6–12]. For example, the concentrations of sodium (Na^+) and potassium (K^+) in sweat normally range from 20–160 mM and 2–16 mM, respectively. Abnormal levels of these electrolytes can lead to several symptoms including hyponatremia, hypokalemia, muscle cramps, dehydration, heat stroke, and in severe cases, even shock (Fig. 1a)[13–15]. Therefore, it is crucial to design and manufacture a low-cost wearable sweat biosensor with excellent performance and large-scale preparation to aid in the prevention and diagnosis of thermal-related diseases.

Wearable sweat ion electrochemical biosensors have gained considerable attention because of their non-invasiveness, in situ continuous monitoring capability, excellent sensitivity, and high specificity[16–22]. These sensors typically consist of three components: (1) a microfluidic layer for capturing, routing and storing sweat, (2) an all-solid-state ion-selective electrode (ISE) for detecting sweat ion concentration changes, and (3) a processing and transmission system of electrical signals[23,24]. Researchers have made great contributions to the multifunctional integration of these components[6–15], but little effort has been devoted to designing new ISEs and improving their performances. The new ISEs are most especially characterized by high stability and high repeatability, because poor stability and repeatability are the main constraints of ISEs in practical applications. Although numerous ISEs have been utilized in the field of sweat monitoring, most studies primarily focus on monitoring changes in electrolyte levels. However, limited research has been conducted to investigate alterations in electrolytes under external interference conditions, such as replenishment of supplemental fluids. In practical applications, it is essential not only to employ wearable sweat sensors for monitoring biomarker fluctuations but also to assess the extent of influence caused by different factors. Therefore, to design a wearable sweat ion electrochemical sensor which is equipped with high sensitivity and reliable stability is of great significance to monitor the changes in human electrolytes under different environments and provide rational guidance for exercise.

The ISE is the core technology of wearable sensors, which determines the authenticity of the detection signal. Typically, an ISE is composed of a conductive substrate, an ion-electron transducer layer and an ion-selective membrane[25]. During prolonged detection, the formation of an interfacial water between the selective membrane and the electrode surface may damage the composition of the selective membrane and cause a

[1]Key Laboratory of Flexible Electronics (KLOFE) & Institute of Advanced Materials (IAM), Nanjing Tech University (Nanjing Tech), Nanjing 211800, China. [2]Department of Neurosurgery, The First Affiliated Hospital of Nanjing Medical University, Nanjing 210029, China. [3]The Institute of Flexible Electronics (IFE, Future Technologies), Xiamen University, Xiamen 361005 Fujian, China. [4]These authors contributed equally: Wenhui Ji, Huanzhuan Liu. ✉email: iamqwu@njtech.edu.cn; iamlli@njtech.edu.cn; iamfwhuo@njtech.edu.cn

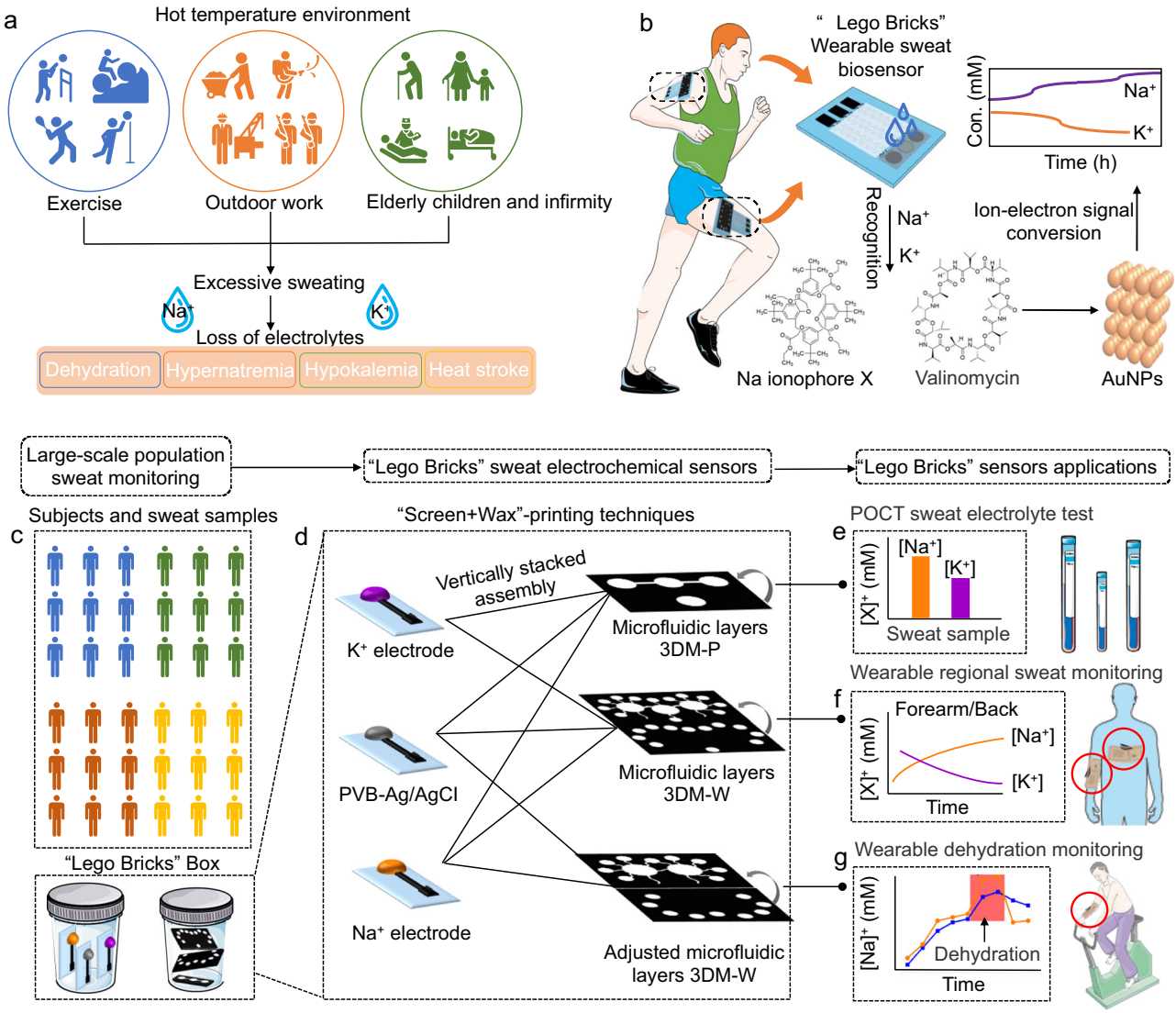

Fig. 1 Schematic diagram of fully printed “Lego Bricks” type wearable sweat sensor for large-scale real-time monitoring Na^+ and K^+. **a** People who engage in physical activities or work in hot environments lose large amounts of Na^+ and K^+ due to excessive sweating, resulting in numerous diseases. **b** Schematic diagram of a wearable sweat sensor for monitoring sweat Na^+ and K^+. **c**, **d** The “Screen+Wax”-printing technology is capable of meeting the demand for large-scale wearable sweat sensing devices in population-level applications. **d** Na^+ and K^+ electrodes and three different designs of microfluidic layers are considered as “building bricks”, which can be taken out of the “Lego Bricks” Box by the users and vertically stacked assembly bricks into different complete devices depending on specific applications. **e**–**g** Three different applications of “Lego Bricks” electrochemical sensors.

potential shift[26]. To address this issue, an ion-electron transducer layer material is usually modified on the electrode surface to improve the potential stability and increase the effective conversion of charge carriers from ions to electrons[27–31]. However, most of the existing ion-electron transducer layer materials are conducting polymers, such as polypyrrole (PPy), which are susceptible to external environmental interference and have poor stability[32,33]. In recent years, metal nanomaterials based on capacitive mechanisms have exhibited superior properties to conducting polymers, including large surface areas, high double capacitance layers, and resistance to external environmental interference[34–37]. Among them, gold nanostructured materials are of great interest due to their excellent biocompatibility, high stability, excellent high double capacitance layers, and controllable preparation[38–40]. For example, Zhang et al. first developed a new ISE for the continuous analysis of sweat Na^+ concentration by using electrodeposition of gold nanodendrites as an ion-electron transducer layer material. However, only the changes of sweat Na^+ were investigated, and the correlation analysis of multiple ions was lacking[41]. This is because the health status is often influenced by multiple biomarkers simultaneously, and therefore, monitoring these biomarkers concurrently can be advantageous to assessing the comprehensive level of health. Niu et al. synthesized monolayer-protected gold nanoclusters (MPCs) and modified MPCs on the electrodes by dropwise addition to prepare a new ISE to investigate its properties. Unfortunately, the synthetic steps were complicated and uncontrollable[42]. Therefore to achieve real-time monitoring and analyze the correlation of multiple sweat ions, there is an urgent need to develop simple and controllable preparation methods to produce ion-electron transducer materials, which can not only exhibit excellent performance but also be ready for large-scale manufacturing.

To prepare flexible electrodes for wearable sweat sensors and microfluidic devices, laser etching, three-dimensional (3D) printing, inkjet printing, and other techniques are usually employed[43–46]. These methods, however, have inherent

limitations including high fabrication costs, tedious steps, and rigid material requirements, which restrict their wide application in the high-throughput preparation of wearable sweat sensors. The sweat-blood biomarkers relationship is still being explored. Therefore, performing large-scale sweat resolution will help to further refine the sweat-blood biomarkers relationship. One of the major obstacles in performing large-scale samples analysis is achieving large-scale fabrication of wearable sweat sensors with high reproducibility, reliable performance, and low cost. Screen printing is a promising high-throughput and cost-effective approach to prepare flexible electrodes with merits such as simple fabrication process and high reproducibility[47]. Since its debut in 2007 by Whitesides et al., paper-based microfluidic device has been extended to various fields such as clinical diagnosis and environmental tests[48,49]. Such device can be constructed by modifying hydrophilic and hydrophobic materials on the paper surface and exploiting the spontaneous capillary effect of paper fibers, which can capture and route of samples without external driving force[50]. In addition, this device can meet the requirements of low-cost and large-scale preparation. Thus, the combination of screen-printing electrodes with wax printing paper-based microfluidic device promises low-cost, homogeneous and reliable mass production of the integrated sensors for large-scale sweat electrolyte analysis during exercise.

Most conventional multifunctional wearable sweat sensors consist of microfluidic layers and sensors that are integrated into a complete device for the detection of multiple biomarkers, including but not limited to simultaneous detection of Na^+, K^+, glucose, lactic acid, uric acid in sweat. However, a challenge arises when the users solely requires the detection of Na^+ and K^+ or exclusively necessitates detection of glucose and lactate without simultaneous assay of other biomarkers, rendering the inclusion of additional functionalities redundant for the users. Here, based on the "Screen+Wax" printing technology, we propose the "Lego Bricks" type of wearable ion electrochemical sensor to monitor sweat Na^+ and K^+ with the advantages of customizable, rapid, large-scale and cost-effective fabrication (Fig. 1). "Lego Brick" refers to the fact that the user can assemble different shapes of building bricks into a desired model according to their needs. Therefore, the term "Lego Brick" wearable sweat sensors specifically refer to the wax-printed paper-based microfluidic layer with various designs, and the screen-printed flexible multifunctional electrodes are utilized as modular components or building bricks (Fig. 1b). The bricks can be assembled vertically to meet the specific requirements of users and form a complete device (Fig. 1c). In this thesis, we utilize sweat Na^+ and K^+ as a monitoring model to showcase the potential application value of the "Lego Brick" wearable sweat sensor. Exercise training induces electrolyte loss of Na^+, K^+, and water in sweat, which can lead to imbalances that impact physical activity. Firstly, the screen-printed carbon electrode surface is modified with controllable hydrophobic gold nanoparticles (AuNPs) as ion-electron transducer layer by a simple one-step electrodeposition method, which exhibits excellent hydrophobicity, favorable electrical properties, reliable stability, and high double-layer capacitance. Then, Na^+ and K^+ selective membranes are modified on the AuNPs layer by dropwise addition, thus completing the preparation of functionalized flexible electrodes. Then, we rapidly and simply construct three foldable 3D microfluidic layers (noted as microfluidic layers 3DM-P, microfluidic layers 3DM-W and adjusted microfluidic layers 3DM-W, respectively) on the paper-based surface by wax-printed technique to realize the capture, route and storage of samples, thus completing the preparation of microfluidic layers. The Na^+ and K^+ electrodes, in conjunction with the three distinct microfluidic layers, can be vertically stacked to create various complete wearable or Point-of-Care Testing (POCT) sensors tailored to specific applications (Fig. 1d). We first select the microfluidic layer 3DM-P and the Na^+ and K^+ electrodes array to assemble the POCT sensor by double-sided adhesive to achieve the determination of Na^+ and K^+ in collected sweat from subjects (Fig. 1e). The test results were compared with standard methods to verify the accuracy of the sensors. Furthermore, we highlight two applications of the "Lego Bricks" wearable sweat sensor. The first is a wearable sweat sensor that integrates microfluidic 3DM-W with Na^+ and K^+ electrodes, enabling the monitoring and analysis of dynamic changes in Na^+ and K^+ levels across different body regions (Fig. 1f). The second involves the integration of the adjusted microfluidic 3DM-W and Na^+ electrodes into a wearable dehydration monitoring sensor, allowing continuous assessment of hydration levels and the impact of various perturbing conditions on hydration status (Fig. 1g). With its rapid high-throughput manufacturability and the capability to analyze multiple electrolytes in sweat, this "Lego Bricks" type wearable sweat ion electrochemical sensor of a modular design is anticipated to serve as a robust analytical tool for exercise and health, presenting a new strategy for large-scale analysis of human sweat metabolites.

RESULTS

Fabrication and characterization of "Lego Bricks" type wearable biosensor

In order to facilitate the modular assembly of various components in the wearable sweat sensor, allowing users to customize their own requirements. Inspired by "Lego Bricks", we prepared a "Lego Bricks" type and mass-producible wearable ion electrochemical biosensor with cost-effectiveness and favorable performance using "Screen+Wax" printing technology, and one-step electrodeposition, which consists of 3D paper-based microfluidic layer and flexible electrodes (Supplementary Fig. 1). Na^+ and K^+ electrode and microfluidics layer are regarded as building bricks in "Lego Bricks" Box that can be assembled into complete devices according to different needs or be easily replaced by new microfluidic layers after testing (Fig. 1c, d). To achieve optimal functionality of the "Lego Bricks" wearable sweat sensor, we employed screen printing and wax printing techniques. These methods are not only scalable, cost-effective, and efficient, but also but also enable easy patterning for diverse shapes and functions of sensors and microfluidic layers. Screen printing technology, on the other hand, was used to ink conductive carbon paste and silver paste on polyethylene terephthalate (PET) substrate (Supplementary Fig. 1a). Then AuNPs were electrodeposited on the working electrode printed with carbon paste, followed by being modified with ion selective membrane of Na^+ and K^+ (Supplementary Fig. 1b) In this way, Na^+ and K^+ can be specifically recognized by Na ionophore X (Na^+) and valinomycin (K^+) and detected by the open-circuit potential test (OCPT) (Fig. 1b). Then, we designed the paper-based microfluidic layer into a two-layer 3D structure by wax printing, which can capture, route and store sweat by its own capillarity without external drive (Supplementary Fig. 1c). Our previously published results demonstrate that the wax covering the paper surface is able to completely penetrate the paper fibers at 100 °C to form a hydrophobic region, so that the samples can only flow along the white hydrophilic region[51]. Specifically, sample permeates through the hydrophilic region of the first layer into the microfluidic channels of the second layer, and then penetrates into the functionalized electrode array. Based on the "Screen +Wax" technology and one-step electrodeposition method, the "Lego Bricks" type wearable electrochemical sensor can not only realize the preparation of stable and excellent ion-electron transducer layer, but also fulfill the demand of large-scale, low-cost and rapid preparation for massive population sweat analysis.

By vertically assembling Na^+ and K^+ electrodes with three different microfluidic layers into three different devices, these

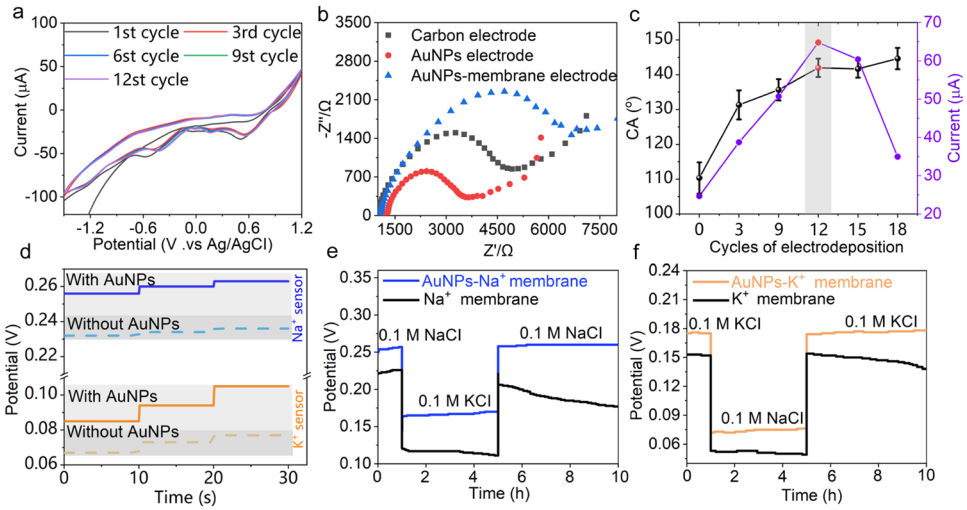

Fig. 2 Characterization of gold nanoparticles as ion-electron transducer layer. a CV curves of electrodeposited AuNPs, potential range: −1.5–1.5 V, scan rate: 50 mV/s, and the number of cycles: 12. **b** EIS of different modified electrodes, 0.01–100000 Hz. **c** CA and reduction peak currents at different electrodeposition cycles. **d** OCPT with/without AuNPs in NaCl or KCl solution. **e**, **f** OCPT of interfacial water of Na^+ ISE and K^+ ISE.

distinct devices can be created for monitoring of Na^+ and K^+ in collected sweat, Na^+ and K^+ in different parts of the body and dehydration. This ultimately confirms the practical value of the "Lego Bricks" wearable or POCT electrochemical sensors. Firstly, to conveniently measure the concentration of Na^+ and K^+ in human sweat collected during exercise, we developed a paper-based microfluidic layer 3DM-P that enables "single-channel sampling, multi-channel simultaneous analysis" (Supplementary Fig. 2), which is combined with Na^+ and K^+ electrodes to create a POCT sensor (Fig. 1e). Secondly, the paper-based microfluidic layer 3DM-W and Na^+ and K^+ electrodes can be assembled into a wearable sweat sensor through the use of a double-sided adhesive layer (Supplementary Fig. 3a, b), with the option to remove the microfluidic layer 3DM-W following a whole cycling test. The microfluidic 3DM-W-based wearable sweat sensor enables simultaneous monitoring of Na^+ and K^+ concentrations changes in different body regions during exercise (Fig. 1f). Thirdly, the adjusted paper-based microfluidic layer 3DM-W and Na^+ electrodes can be integrated into a wearable dehydration monitoring device (Supplementary Fig. 3a, c), enabling the assessment of dehydration symptoms during prolonged exercise and the evaluation of different interferences on dehydration (Fig. 1g). In general, the microfluidic layers not only effectively conform the human skin surface and minimize its contact with the electrode surface materials to prevent discomfort, but also significantly reduce sweat evaporation, pollution, and accumulation. Additionally, the electrodes are rinsed with ultrapure water and integrated with a new microfluidic layer to construct a new "Lego Bricks" wearable sensor for subsequent testing. The findings suggest that the "Screen+Wax" printing technology not only enables the fabrication of low-cost, large-scale, rapid, and easily patterned microfluidic layers and electrode arrays, but also allows for arbitrary assembly of devices into various "Lego Bricks" electrochemical biosensors.

Characterization of gold nanoparticles as ion-electron transducer layer

When the deposition potential is lower than the standard electrode potential of 0.78 V (vs. Ag/AgCl) for the $AuCl_4^-$/Au electrode pair, $AuCl_4^-$ can be reduced to Au atoms and continue to accumulate into AuNPs. As shown in Fig. 2a, the redox peaks appearing at about 0.6 V and 1.0 V indicate that $AuCl_4^-$ is successfully reduced to Au atoms. The reduction peaks after the second cycle shift to a more positive potential, which represents the preferential electrodeposition of gold on the previously deposited gold nuclei[52,53]. Then, we characterized the layer-by-layer modification process of the electrode in potassium ferricyanide using electrochemical impedance spectroscopy (EIS). The charge transfer resistance (R_{ct}) of the electrode modified with AuNPs (named AuNPs electrode) is smaller than that of the carbon electrode, indicating that the deposited AuNPs are able to accelerate the electron transfer efficiency. The R_{ct} gets higher when the Na^+ selective membrane (named AuNPs-membrane electrode) is further modified, suggesting that ion-selective membrane is less a conductive material but more an ion detector (Fig. 2b). The contact angle (CA), scanning electron microscopy (SEM), and cyclic voltammetry (CV) test results demonstrate that the optimal electrodeposition cycles are 12 (Supplementary Fig. 4). Specifically, the CA test suggests that the hydrophobicity of the electrode surface reaches 141° at the 12th electrodeposition cycle, and thereafter remains almost constant with increasing electrodeposition cycles (Fig. 2c). As shown in the transmission electron microscope (TEM) images, with the increase of electrodeposition cycles, new particles preferentially grow on the preformed AuNPs. Then, AuNPs gradually become larger in size. The small-scale aggregation of AuNPs on the electrode surface is observed at the 18th cycle (Supplementary Fig. 4). The CV test indicates the maximum reduction peak current to be 65 μA at the 12th cycle, suggesting the largest electrochemical surface area (ECSA) at this point (Fig. 2c). The ECSA (A) of different electrodes is calculated from CV curves using the Randles–Sevick equation[54]:

$$I_{pa} = 2.69 \times 10^5 \times AD^{\frac{1}{2}} n^{\frac{3}{2}} \gamma^{\frac{1}{2}} C$$

where n is the number of electrons contributing to the redox reaction and is equal to 1. D represents the diffusion coefficient of the redox probe $(6.7 \pm 0.02) \times 10^{-6}$; C is the concentration of the redox probe (mol/L, 5 mM); I_{pa} is the anode peak current (A); and γ is the scan rate (V/s, 50 mV/s). All peak anode currents are obtained from CVs and the calculated ECSAs are listed in Supplementary Table 1. A of the bare carbon electrode is 1.4×10^{-5} cm^2 and that for 12 cycles is 7.0×10^{-5} cm^2. All these results demonstrate that AuNPs have faster electron transfer rate and higher ECSA than bare electrode. Although the prolonged electrodeposition cycles may increase the amount of AuNPs, excessive AuNPs can lead to aggregation and form clusters on the electrode surface, further decreasing the specific surface area and the current (Supplementary Table 1)[55].

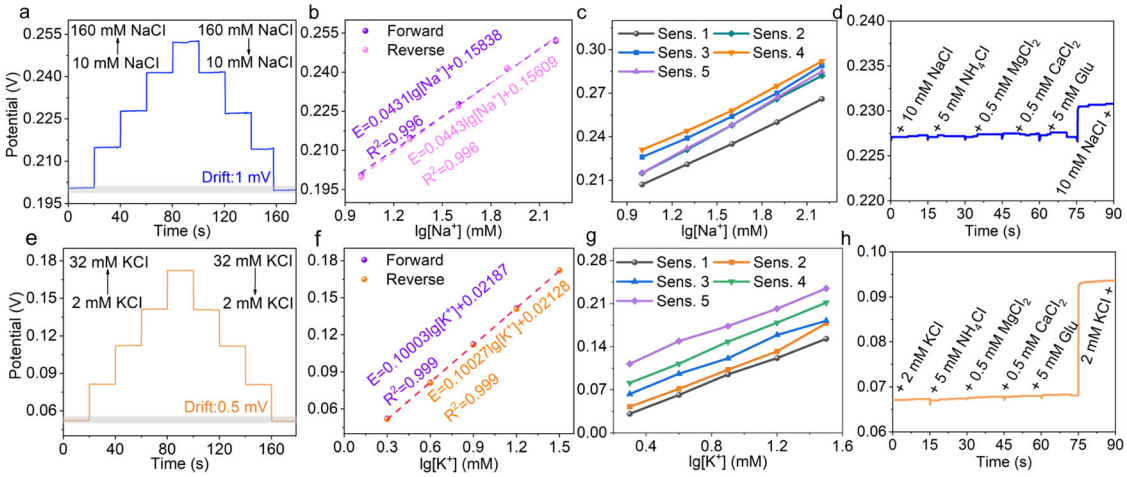

Fig. 3 Characterization of in vitro sodium and potassium ion sensors. a OCPT response and hysteresis test of Na^+ sensor in NaCl solution, **b** forward and reverse calibration plots, **c** reproducibility test, and **d** selectivity test. **e** OCPT response and hysteresis test of K^+ sensor in KCl solution, **f** forward and reverse calibration plots, **g** reproducibility test, and **h** selectivity test.

Energy dispersive spectroscopy (EDS) analysis shows the characteristic peak of gold atoms at around 2.18 keV, indicating the successful electrodeposition of AuNPs on the carbon electrode (Supplementary Fig. 5). Furthermore, a comparison was made between electrodes modified and unmodified with AuNPs in NaCl or KCl solutions. It is found that the potential of the ISEs modified AuNPs increased significantly, indicating that AuNPs can improve the ion-electron transfer efficiency between the ion-selective membrane and the conducting substrate (Fig. 2d). The interfacial water layer of the prepared electrodes was evaluated using a standardized experimental procedure[56]. In 0.1 M KCl solution, both electrodes (AuNPs-Na^+ membrane and Na^+ membrane) exhibit a significant potential reduction (Fig. 2e). The potential of the electrode modified with only Na^+ membrane decreases after a period of stabilization, while that of the AuNPs-Na^+ membrane electrode remains stable. When returned to 0.1 M NaCl solution again, the AuNPs-Na^+ membrane electrode maintains the initial potential value with no noticeable potential drift, whilst the Na^+ membrane electrode shows a significant potential decrease. Similar experimental results are obtained for the electrode modified AuNPs-K^+ membrane (Fig. 2f). The above findings lead us to conclude that the AuNPs prepared by a simple one-step electrodeposition method not only possess hydrophobic properties to effectively avoid the emergence of interfacial water, but also ensure the excellent stability and electrical properties of the electrodes.

Characterization of in vitro sodium and potassium ion sensors

Fast and convenient monitoring of Na^+ and K^+ was achieved by using ISE modified ion-selective membrane and reference electrode modified PVB. AuNPs were used as ion-electron transducer layer materials, while multi-walled carbon nanotubes were incorporated in PVB membrane to achieve stable potential output and reduce potential drift during long-term continuous monitoring. Compared with carbon and AuNPs electrodes, the morphology of electrodes modified with Na^+ and K^+ selective membranes show evident and complete changes, reflecting the successful modification of the ion-selective membranes on the electrode surface (Supplementary Fig. 5b, c). In addition, we optimized the volume of the ion selective membrane for better sensor sensitivity and response time. The optimal volume of the Na^+ and K^+ selective membranes is 0.1 and 0.12 μL/mm^2, respectively (Supplementary Fig. 6). As shown in Fig. 3a, b, the potential response of the Na^+ sensor in 10–160 mM NaCl is consistent with the analyte concentration variation, and its hysteresis value is approximately 1 mV. The sensitivity values before and after the reversible response are 43.1 and 44.3 mV/decade, respectively, reflecting superior reversibility. Furthermore, the reproducibility test of the Na^+ sensor displays highly consistent sensitivity (Fig. 3c). But the potential values of ISE in the same solution are different, possibly caused by the subtle differences in the manufacturing process. To address this issue, we adopted a single-point calibration method in which the sensor was calibrated in 10 mM NaCl solution before each test. Its potential value is recorded as 0 V, and then a single-point calibration linear fit is obtained with a sensitivity of 54.29 mV/decade (Supplementary Fig. 7a). As for the selectivity test, different interferents normally available in sweat are selected (Fig. 3d and Supplementary Fig. 8a). Note that these interferents, in fact, do not interfere the response potential at all, and the sensor exhibits excellent specificity. Figure 3e, f display the potential response of the K^+ sensor in 2-32 mM KCl and its hysteresis test. Similarly, the response potential value increases (decreases) gradually with augmenting (reducing) the analyte concentration. The hysteresis value is around 0.5 mV and the sensitivity values before and after the reversible response are 100.03 and 100.27 mV/decade, respectively, exhibiting excellent reversibility and rapid recovery. Likewise, the reproducibility test of exhibits a high consistency of sensitivity. The single-point calibration method was also adopted in K^+ sensor, which was calibrated in 2 mM KCl before each test with the potential value being recorded as 0 V. The single-point calibration linear fit is obtained with a sensitivity of 102.5 mV/decade (Supplementary Fig. 7b). The selectivity test of K^+ sensor in Fig. 3h and Supplementary Fig. 8b also demonstrates that it is not affected by other common interferents found in sweat. All the above behaviors manifest the favorable electrochemical performance of the prepared AuNPs-based wearable ion biosensors.

Characterization of mechanical deformation and stability of wearable sensors

Since wearable sensors are often subjected to mechanical deformation such as bending or twisting for practical application, the mechanical deformation performance of the prepared wearable sensor should be investigated. Note that as the PET material is rarely stretched, we did not study the stretchability of the sensor. The resistance of the AuNPs-modified electrode is consistently stable at approximately 155 Ω during bending from 0 to 180° with a relative standard deviation (RSD) of 0.52% (Supplementary Fig. 9). Then, we examined the potential changes

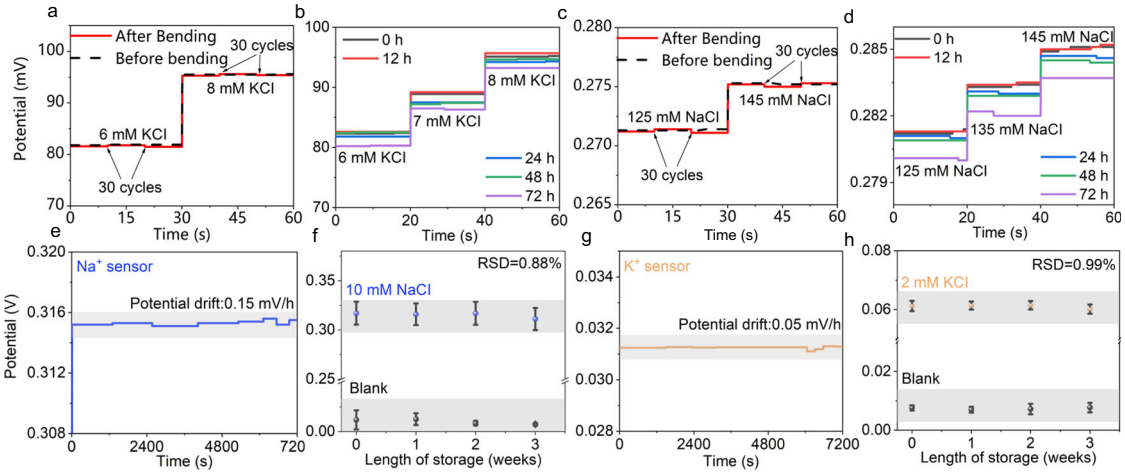

Fig. 4 Mechanical deformation characterization, corrosion resistance characterization and sensor stability of wearable sensors. OCPT response of Na^+ (**a**) sensor and K^+ (**c**) sensor under different bending times. Corrosion resistance measurements of Na^+ (**b**) sensors and K^+ (**d**) sensors immersed in artificial sweat. **e**, **g** The long-term test stability of the sensors, and the voltage drift values of the Na^+ and K^+ sensors were 0.15 mV/h and 0.05 mV/h, respectively, after 3 h of continuous testing. **f**, **h** the long-term storage stability of the sensors, respectively, and the prepared sensors were stored in a refrigerator with lightproof sealing at 4 °C and tested at weeks 0, 1, 2, 3, respectively ($n = 3$). The error bars represent the standard deviations of the measured data.

of the Na^+ and K^+ sensors before and after bending (Fig. 4a, c). The results show that negligible potential changes are observed even after 30 times of bending (compared to before bending), indicating their ability to resist mechanical deformation. Next, the corrosion resistance of the sensors was evaluated by immersing them in artificial sweat. Compared to 0 h, there is no significant fluctuation in potential within 48 h. An obvious potential decrease is recorded after 72 h of immersion, which may be attributed to the detachment or corrosion of the material on the electrode (Fig. 4b, d). In addition, the long-term stability and storage stability of the sensors were also explored. During the two-hour stability test, the potential drifts of the Na^+ and K^+ sensors are 0.15 and 0.05 mV/h, respectively (Fig. 4e, g). In the three-week storage stability test, the RSDs of the Na^+ and K^+ sensors are 0.88% and 0.99%, respectively (Fig. 4f, h). Overall, the prepared sensors have better resistance to mechanical deformation and corrosion, which provides a guarantee for the subsequent monitoring of electrolyte changes during human exercise.

Analysis of Na^+ and K^+ concentration in sweat from different parts of the body

Dynamic in situ real-time monitoring of sweat Na^+ and K^+ changes during exercise can provide important scientific guidance and health protection for field training. The paper-based microfluidic 3DM-W and Na^+ and K^+ electrodes are integrated into a modular "Lego Bricks" wearable sweat sensor, enabling dynamic and continuous monitoring of forearm and back sweat Na^+ and K^+ levels during exercise (Fig. 5a). This facilitates the analysis of electrolyte trends across different body regions. The optical photograph of subjects wearing wearable sensors on their forearm and back are shown in Fig. 5b. Before conducting the cycling test, we determine the sensitivities S1 and S2 of Na^+ and K^+ sensors in standard solutions, respectively. Subsequently, these sensors are applied to the subject's arm during exercise. After the test, we individually measure sensitivities S3 and S4 for the same Na^+ and K^+ sensors. Comparison with previous results indicate that sensor sensitivity remains unaffected before and after the exercise (Supplementary Fig. 10a, b). The ex-situ detection data (dots) and real-time monitoring data (curves) of Na^+ and K^+ under constant exercise speed overlap completely, indicating the feasibility of the prepared sensor for practical application (Fig. 5c). The scatter fit plots of Na^+ and K^+ ex-situ and on-body, exhibit Pearson coefficients of 0.97 and 0.87, respectively, indicating a better correlation and accuracy (Fig. 5d). To further validate the accuracy of the sensor, the sweat collected during exercise is diluted and subsequently analyzed using inductively coupled plasma optical emission spectrometry (ICP-OES) and microfluidic layer 3DM-P, along with Na^+ and K^+ electrodes integrated into a POCT sensor, respectively (Supplementary Fig. 10c). The aforementioned outcomes are subsequently compared with those of the POCT sensor, revealing their approximate congruence and thereby attesting to the sensor's high precision. (Supplementary Fig. 10d). The whole exercise process can be divided into three stages: high intensity (25 km/h), low intensity (15 km/h) and rest (Fig. 5e). The real-time curves of sweat Na^+ and K^+ show that as exercise intensity increases and then decreases, the Na^+ concentration increases and then gradually becomes steady in the three subjects, while K^+ concentration gradually decreases and then stabilizes (Fig. 5f, g). During high-intensity exercise, the higher sweat rate and lower reabsorption efficiency lead to higher sweat Na^+ concentration, mainly because the concentration of sweat Na^+ is positively correlated with the sweat rate[57]. During low-intensity exercise, the lower sweat rate reduces the sweat Na^+ concentration. However, sweat K^+ is proportional to blood K^+ concentration rather than positively correlated with sweat rate[58]. During high-intensity exercise, the large amount of secreted sweat dilutes the blood K^+ concentration, which in turn causes the sweat K^+ concentration to decrease. As exercise decreases, sweat K^+ concentration exhibits a relatively stable trend, essentially due to its passive ion partitioning mechanism[58]. Moreover, we process the data in Fig. 5f, g and obtained results in Fig. 5h, i. By comparing the forearm and back Na^+ concentrations at the 20th, 30th, and 40th minutes, we find that Na^+ concentration in the back is generally slightly higher than that in the forearm, mainly attributed to the high density of sweat glands and high sweating rate in the back[57]. Similarly, the differences of K^+ concentrations from forearm and back are analyzed. As shown in Fig. 5h, i, the back K^+ concentration is slightly higher than the forearm at the beginning of exercise, but eventually remains at similar levels. The slight difference is caused by the regular internal potassium balance which maintains an asymmetric distribution of the total body potassium content between intracellular and extracellular fluids. The trends of Na^+ and K^+ changes are the same in the back and forearm,

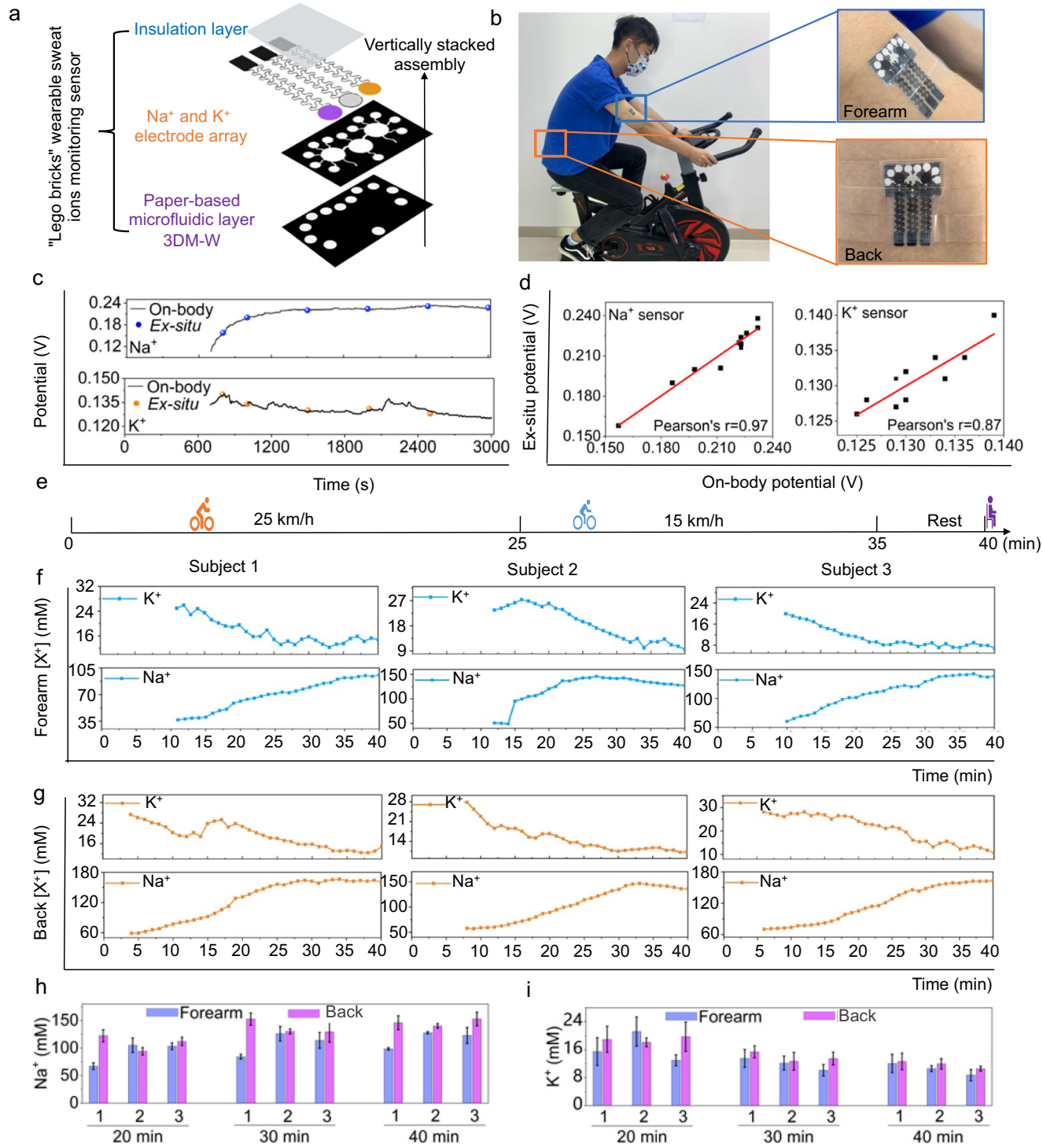

Fig. 5 Analysis of sodium and potassium ions in sweat from different parts of the body. a Schematic of the vertically assembled "Lego Bricks" wearable sweat ion sensor. **b** Optical photographs of "Lego Bricks" wearable ion sensor worn on the forearm and back of the subject. Consent was obtained for publication of the photograohs. **c** The same wearable sweat ion sensor enables real-time on-body monitoring and ex-situ collection measurement of sweat. **d** Scatter fit plots of on-body and ex-situ Na^+ and K^+ detection. **e** The exercise process is divided into three phases: high intensity, low intensity, and rest. **f** Temporal changes in sweat Na^+ and K^+ concentration in the forearm during exercise, and (**g**) sweat Na^+ and K^+ concentration in the back during exercise. Analysis of (**h**) Na^+ and (**i**) K^+ concentrations in the back and forearm at different time of exercise ($n = 3$). The error bars represent the standard deviations of the measured data.

but the lower sweating rate of the forearm delays the activation of the sensor for a while. The above results reveal that the back is more ideal for sweat monitoring. However, considering the ion concentration differences between the forearm and the back are insignificant, we chose the forearm for the next prolonged exercise monitoring from the perspective of practicality and convenience. Furthermore, future research can incorporate sweat rate measurement into "Lego Bricks" wearable sweat sensors, thereby facilitating the prediction of overall electrolyte loss through monitoring localized electrolyte levels in the body.

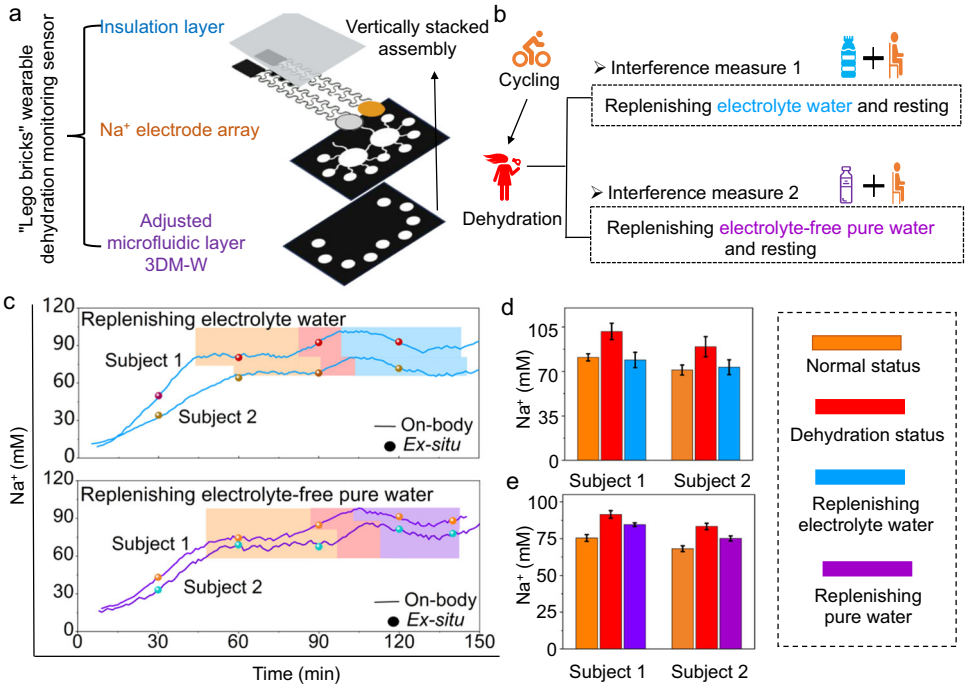

Fig. 6 Real-time monitoring of electrolytes during prolonged exercise and the influence of different interventions. a Schematic diagram of the layered assembly structure of the "Lego Bricks" wearable dehydration monitoring sensor. **b** Two different interference measures are taken to influence the dehydration that occurs in subjects during prolonged exercise. **c** Real-time change curve of Na^+ concentration of subjects during approximately 150 min exercise (top: subjects supplementing with electrolyte water. Bottom: subjects supplementing with electrolytes-free pure water). **d** Changes in Na^+ concentration before and after electrolyte water supplementation and (**e**) electrolyte-free pure water when subjects are dehydrated ($n = 3$). The error bars represent the standard deviations of the measured data.

Real-time monitoring of electrolytes during prolonged exercise and the influence of different interventions

Maintaining electrolyte balance is critical to human health, especially in scenarios such as field training and racing, where excessive electrolyte loss can lead to electrolyte disorders. Real-time dynamic monitoring of electrolyte changes can help supply proper fluid replacement to maintain normal body functions. Sweat Na^+ serves as the indicators of human body dehydration[59]. Since only the concentration of Na^+ is to be monitored, we developed a "Lego Bricks" wearable sweat sensor using a modular approach, integrating the Na^+ electrode and adjusted microfluidic layers 3DM-W to meet practical application requirements. This innovative design enables accurate monitoring of dehydration during prolonged exercise and facilitates assessment of dehydration status through various interference measures (Fig. 6a). During constant cycling, the Na^+ concentration initially increases, suggesting the possibility of dehydration. Then the subjects were offered different supplemental liquids (electrolyte water and pure water) to alleviate dehydration. The cycling activity was resumed following a brief intermission to examine the dehydration condition of the participants (Fig. 6b). The exercise rate is constant, the concentration of Na^+ initially increases and then gradually becomes stable as the duration of exercise prolongs. At around 90 min, the Na^+ concentration of subjects 1 and 2 increases, indicating dehydration (red block). Subjects 1 and 2 exhibit dehydration upon an increase in their Na^+ concentrations from approximately 80 and 67 mM to 100 and 80 mM, respectively (Fig. 6c). This is because dehydration-induced hemoconcentration increases the concentration of extracellular Na^+, which ultimately results in a slight increase in sweat Na^+[58]. At this time, subject 1 were supplemented with electrolyte water and rested momentarily. The Na+ concentration remains stable for a certain duration and gradually decreases and eventually returns to the normal level (blue block), with the entire process lasting approximately 40–50 min (Fig. 6d). Electrolyte water replenishes the body with essential ions and facilitates evaporative cooling during rest, resulting in a reduction in Na^+ concentration. By providing subject 2 with pure water without electrolytes during the period of rising Na^+ concentrations and allowing them to rest for an equal duration before cycling again, the concentration of Na^+ is reduced but fails to return to normal levels. (Fig. 6c, e). Therefore, electrolyte water is better than pure water for relieving dehydration, but appropriate supplementation should be considered to prevent other adverse reactions caused by excessive water consumption. In this study, we have conducted preliminary experiments to demonstrate the potential of "Lego Bricks" wearable sweat sensors in monitoring dehydration and evaluating its impact under various perturbing conditions. Future investigations should also incorporate sweat rate monitoring, along with large-scale studies involving multiple experimental groups and rigorous statistical analysis, to comprehensively assess dehydration.

DISCUSSION

In this work, we have proposed a ready-to-use, large-scale, arbitrarily assembled, and fully printed "Lego Bricks" type wearable ion electrochemical sensor based on hydrophobic AuNPs and ion selective membranes. The sensor comprises printed flexible ion electrodes and paper-based microfluidic layers using "Screen+Wax" printing techniques, which are cost-effective, homogeneous, and high-throughput. AuNPs are prepared using a simple one-step electrodeposition method with hydrophobicity, high capacitance, and excellent electrical properties. Finally, we modify Na^+ and K^+ selective membranes on the electrode modified AuNPs to produce fully printed flexible ion-selective electrodes.

To enable users to customize the assembly of wearable sweat sensor modules based on their specific requirements, we have introduced a modular approach inspired by the concept of "Lego Bricks". Specifically, "Lego bricks" electrochemical sensors comprise screen-printed flexible electrodes and wax-printed paper-based microfluidic layers, which are treated as distinct modules within a "Lego Bricks" Box. Users can selectively choose and vertically integrate these modules to create a fully functional wearable sweat sensor. To validate the concept of the "Lego Bricks" sensor, we designed and prepared three microfluidic layers (3DM-W, 3DM-P and adjusted microfluidic layer 3DM-W), and two ion selective electrodes (Na^+ and K^+). Firstly, we integrated microfluidic layer 3DM-P and two ion electrodes into a POCT sensor for the determination of Na^+ and K^+ in sweat collected during exercise. The accuracy of the prepared sensor was demonstrated by comparison with the standard method ICP-OES. Then, we combined the microfluidic layer 3DM-W and the two ion electrodes into a "Lego Bricks" wearable sweat sensor to monitor and analyze the sweat Na^+ and K^+ from different body regions during exercise. The results showed that sweat Na^+ concentration initially increases and then stabilizes while K^+ concentration firstly reduces and then gradually stabilizes. The Na^+ concentration of the back was slightly higher than the forearm, while the final concentration of K^+ in the back and forearm remained at approximately the same levels, which may be because Na^+ was affected by the sweat rate while K^+ was independent of it. Finally, we customized the microfluidic layer 3DM-W to facilitate the monitoring of the dehydration indicator (Na^+ concentration) during prolonged exercise while assessing the effect of pure water and electrolyte water supplementation on dehydration. The preliminary experimental results suggest that electrolyte water is more effective against dehydration.

In the future, we plan to introduce genomic studies to establish a personalized "Gene-Sweat-Disease" spectrum to comprehensively analyze the correlation between sweat metabolites and physiology. Additionally, the direct complexion of ion-electron transducer layer materials with ion-selective membranes will be explored to further boost the fabrication throughput of sweat sensors. Furthermore, the development of more functional electrodes such as those for glucose, uric acid, dopamine, cortisol and sweat rate measurement, along with versatile microfluidic layers will enhance the applicability of the "Lego Bricks" wearable sweat sensor. Additionally, incorporating traditional Chinese mortise and tenon structure in device design will facilitate universal assembly of these sensors. We believe that the "Lego Bricks" wearable sweat biosensor will be a powerful tool for personalized health diagnosis, contributing to the plotting of a comprehensive exercise health map.

METHODS

Chemicals and materials

PET (20 × 30 cm) was purchased from Xfnano Co. (Nanjing, China). Whatman chromatography paper #1 (20 × 20 cm) was purchased from GE Healthcare Worldwide (Shanghai, China). The carbon ink and silver ink were purchased from Shenzhen D-MAX technology Co. Ltd. (Shenzhen, China). $FeCl_3$, $HAuCl_4$ (1%), Na_2SO_4, NaCl, KCl, NH_4Cl, $MgCl_2$, $CaCl_2$, glucose, $[Fe(CN)_6]^{3-}$, $[Fe(CN)_6]^{4-}$, bis(2-ethylehexyl) sebacate (DOS), sodium tetrakis[3,5-bis(trifluoromethyl)phenyl] borate (Na-TFPB), high-molecular-weight polyvinyl chloride (PVC), tetrahydrofuran, valinomycin, sodium tetraphenylborate (NaTPB), cyclohexanone, polyvinyl butyral resin BUTVAR B-98 (PVB), and multiwall carbon nanotubes were purchased from Aladdin (Shanghai, China). Selectophore grade sodium ionophore X was obtained from Sigma Aldrich (Shanghai, China). Block polymer PEO-PPO-PEO (F127) was obtained from Energy Chemical (Shanghai, China). Artificial sweat (pH 6.0) was obtained from Yuanye Bio-Technology Co., Ltd (Shanghai, China). Deionized water (18.2 MΩ cm) was obtained from a Milli-Q water purification system.

Instruments

Electrochemical measurements were carried out on PalmSens 4.0 electrochemistry system of Palm Instruments (The Netherlands). The microscopic morphology of the sample was characterized by JSM-7800F field emission scanning electron microscopy (FE-SEM). Wax printing was performed by Xerox ColorQube 8570 wax printer. Contact angle was characterized by KRUSS GmbH (DSA1005). Stretch test was conducted by universal testing machine ESM303 (EUCHNER GmbH). The gold standard test method for sweat samples was characterized by inductively coupled plasma optical emission spectrometry (ICP-OES) (Perkin Elmer Avio 200).

Design and fabrication of flexible electrodes by screen-printing method

The process of fabricating the flexible electrodes were illustrated in Fig. S1. The patterns of the flexible electrodes were designed by AutoCAD. The PET substrate was first ultrasonically cleaned with ultrapure water, ethanol and ultrapure water, respectively, and then the PET surface was blown dry with nitrogen gas. Conductive carbon ink was used as the working electrode (WE) and counter electrode (CE), and conductive silver ink was used as the reference workd (RE). The printing ink was printed on the PET substrate by screen printing template. After printing, the screen-printing electrodes were dried at 150 °C in oven for 15 min. Ag/AgCl was then formed by dropping 50 mM $FeCl_3$ onto the RE surface for about one minute.

Functionalization of flexible electrode array

(1) Electrodeposition of gold nanoparticles. The screen-printing electrodes were pretreated in 50 mM H_2SO_4 solution using CV by sweeping the potential from −0.4–1 V at 100 mV/s for 10 cycles with an external Pt counter electrode and Ag/AgCl reference electrode. The pretreated screen-printing electrodes were placed in 0.1% $HAuCl_4$ in 0.5 M Na_2SO_4 solution for electrodepositing using CV method from −1.5–1.5 V at 50 mV/s for 12 cycles with an external Pt counter electrode and Ag/AgCl reference electrode. After electrodeposition, the electrode surface was rinsed with ultrapure water to remove the residual $HAuCl_4$ solution.

(2) Preparation of Na^+ working electrode. The Na^+ selective membrane cocktail solution was prepared by dissolving 10.0 mg Na ionophore X, 5.5 mg Na-TFPB, 330.0 mg PVC and 664.4 mg DOS in 6.6 ml tetrahydrofuran. The prepared Na^+ selective membrane cocktail solution was dropped onto the surface of the WE modified AuNPs in the volume of 4 µL, 4 µL sequentially. The modified WE was then dried overnight.

(3) Preparation of K^+ working electrode. The K^+ selective membrane cocktail solution was prepared by dissolving 20.0 mg valinomycin, 5.0 mg NaTPB, 327.0 mg PVC and 656.8 mg DOS in 6.6 mL cyclohexanone. The prepared K^+ selective membrane cocktail solution was dropped onto the surface of the WE modified AuNPs in the volume of 4 µL, 4 µL, 2 µL sequentially. The modified WE was then dried overnight.

(4) Preparation of PVB reference electrode. The solution for the PVB reference electrode was 79.1 mg PVB, 50 mg NaCl by dissolving in 1 mL methanol solution, and then 2 mg F127. Next, 0.2 mg of multi-walled carbon nanotubes were

dissolved in the above solution to reduce the potential shift. The prepared PVB solution was dropped onto the surface of the RE in the volume of 4 µL, 4 µL, 2 µL sequentially. The modified RE was then dried overnight.

Design and preparation of 3D paper-based microfluidic layers

The process of preparing a 3D paper-based microfluidic layer was shown in Supplementary Figs. 1c, 2 and 3. The microfluidic layer was designed by AutoCAD, where the black area is hydrophobic, and the white area is hydrophilic (Supplementary Fig. 1c). The preparation procedure is referred to our previously published article[51]. Briefly, the hydrophobic region is covered by wax on the paper-based surface by Xerox ColorQube 8570 wax printer. Then the paper is baked in 100 °C for 2 min to facilitate the wax penetration into the paper fibers to form the hydrophobic region. Finally, the prepared double-layer microfluidic device is simply folded. Laser cutting technology was employed to fabricate diverse designs of adhesive layers on double-sided adhesive, followed by vertical bonding and assembly with paper-based microfluidic layers to achieve a fully integrated microfluidic layers (Supplementary Figs. 2, 3). Sweat on the skin surface can penetrate through the white hydrophilic zone of the first layer into the channels of the second layer, where there is a perspiration outlet that prevents sweat from accumulating in the second microfluidic layer.

Electrochemical characterization of wearable sensor

Electrochemical characterization was performed by PalmSens 4.0 electrochemistry system of Palm Instruments (The Netherlands). CV and EIS were performed by a three-electrode system in 5 mM $[Fe(CN)_6]^{3-}$/$[Fe(CN)_6]^{4-}$ and 0.1 M KCl solution, which used Pt counter electrode and Ag/AgCl reference electrode. OCPT was performed in different solutions using a two-electrode system.

Off-body sweat analysis

Before starting the test, the test body parts of subjects were wiped with alcohol and deionized water, respectively, and then the wearable sensors were attached to the test regions *via* 3 M medical tape. Subjects were trained to cycle at 25–30 °C and sweat at different time during the test was collected into centrifuge tubes via straws and then stored in a −20 °C refrigerator. After subjects complete a complete cycling test, the microfluidic layer was removed and the electrode array was rinsed with ultrapure water and blown dry with N_2. The new microfluidic layer was then reassembled with the electrode array to form a new wearable sensor to be placed in the 4 °C refrigerator for the next use.

ICP-OES determination of collected sweat samples

First, subjects performed a 20 km/h cycling test for approximately 30 min, during which sweat was collected with the pipette and stored in a 0.5 mL centrifuge tube. The method for sweat dilution was referenced from a published work on ICP determination of biological samples and further improved[60]. The sweat samples were diluted using the direct dilution method. 0.3 mL of sweat was mixed with 9.7 mL of 0.1% HNO_3 and then centrifuged at 3500 rpm for 10 min, and the supernatant was used as the test sample.

ICP-OES standard curves were plotted. The mixed solutions of NaCl and KCl with final concentrations of 0.005 mg/mL, 0.025 mg/mL, and 0.1 mg/mL were prepared with 0.1% HNO_3, respectively. Then the standard curves were determined by ICP-OES.

On-body sweat analysis

To investigate the performance of the prepared wearable sweat ion electrochemical sensor for practical exercise monitoring, we performed sweat ion analysis during indoor exercise in three healthy volunteers aged 22–27 years at 25–30 °C. Before the experiment, the subjects' forearm and back were individually cleaned with alcohol. The prepared wearable sensors were attached to different skin areas with waterproof medical tape and connected to a portable PalmSens electrochemical workstation. Subjects were required to wear the wearable device for cycling at different intensities to monitor the changes of sweat Na^+ and K^+ during exercise.

The wearable biosensors should be calibrated before and after the measurements to avoid potential changes that could affect the signal readings after exposure to the sweat samples. At the end of the cycling, real-time concentrations of sweat Na^+ and K^+ during exercise were obtained from the calibration curve calculations.

Written informed consent was obtained, and the studies involving human participants were reviewed and approved by Institutional Ethics Committee of The First Affiliated Hospital of Nanjing Medical University. Photographs used were obtained with subject's consent.

DATA AVAILABILITY

All data are available within the article or available from the authors upon reasonable request.

Received: 1 April 2023; Accepted: 24 November 2023;
Published online: 20 December 2023

REFERENCES

1. Broza, Y. Y. et al. Disease detection with molecular biomarkers: from chemistry of body fluids to nature-inspired chemical sensors. *Chem. Rev.* **119**, 11761–11817 (2019).
2. Mohan, A. M. V., Rajendran, V., Mishra, R. K. & Jayaraman, M. Recent advances and perspectives in sweat-based wearable electrochemical sensors. *Trac-Trends Anal. Chem.* **131**, 116024 (2020).
3. Ji, W. et al. Wearable sweat biosensors refresh personalized health/medical diagnostics. *Research* **2021**, 9757126 (2021).
4. Ghaffari, R. et al. State of sweat: emerging wearable systems for real-time, non-invasive sweat sensing and analytics. *ACS Sens.* **6**, 2787–2801 (2021).
5. Wang, L. et al. Skin-like hydrogel-elastomer based electrochemical device for comfortable wearable biofluid monitoring. *Chem. Eng. J.* **455**, 140609 (2023).
6. Sempionatto, J. R. et al. Wearable chemical sensors for biomarker discovery in the omics era. *Nat. Rev. Chem.* **6**, 899–915 (2022).
7. Manjakkal, L., Yin, L., Nathan, A., Wang, J. & Dahiya, R. Energy autonomous sweat-based wearable systems. *Adv. Mater.* **33**, 2100899 (2021).
8. Kim, J., Campbell, A. S., de Ávila, B. E. F. & Wang, J. Wearable biosensors for healthcare monitoring. *Nat. Biotech.* **37**, 389–406 (2019).
9. Wang, L. et al. A core-sheath sensing yarn-based electrochemical fabric system for powerful sweat capture and stable sensing. *Adv. Funct. Mater.* **32**, 2200922 (2022).
10. Xiao, J. Y., Fan, C., Xu, T. L., Su, L. & Zhang, X. J. An electrochemical wearable sensor for levodopa quantification in sweat based on a metal-organic framework/graphene oxide composite with integrated enzymes. *Sens. Actuators B-Chem.* **359**, 131586 (2022).
11. Wang, J. et al. Ultra-small wearable flexible biosensor for continuous sweat analysis. *ACS Sens.* **7**, 3102–3107 (2022).
12. He, X., Fan, C., Luo, Y., Xu, T. & Zhang, X. J. Flexible microfluidic nanoplasmonic sensors for refreshable and portable recognition of sweat biochemical fingerprint. *npj Flex. Electron* **6**, 60 (2022).
13. Gao, W. et al. Fully integrated wearable sensor arrays for multiplexed in situ perspiration analysis. *Nature* **529**, 509–514 (2016).
14. He, X. et al. Integrated smart janus textile bands for self-pumping sweat sampling and analysis. *ACS Sens.* **5**, 1548–1554 (2020).
15. He, X., Fan, C., Xu, T. & Zhang, X. J. Biospired janus silk e-textiles with wet–thermal comfort for highly efficient biofluid monitoring. *Nano Lett.* **21**, 8880–8887 (2021).
16. Wu, W. et al. Optical flexible biosensors: from detection principles to biomedical applications. *Biosens. Bioelectron.* **210**, 114328 (2022).
17. Wang, Y. et al. Wearable plasmonic-metasurface sensor for noninvasive and universal molecular fingerprint detection on biointerfaces. *Sci. Adv.* **7**, eabe4553 (2021).

18. Wang, M. Q. et al. A wearable electrochemical biosensor for the monitoring of metabolites and nutrients. *Nat. Biomed. Eng.* **6**, 1225–1235 (2022).
19. Chen, L. et al. Superhydrophobic functionalized Ti_3C_2Tx MXene-based skin-attachable and wearable electrochemical pH sensor for real-time sweat detection. *Anal. Chem.* **94**, 7319–7328 (2022).
20. Yang, Y. et al. A laser-engraved wearable sensor for sensitive detection of uric acid and tyrosine in sweat. *Nat. Biotech.* **38**, 217–224 (2020).
21. Sempionatto, J. R. et al. An epidermal patch for the simultaneous monitoring of haemodynamic and metabolic biomarkers. *Nat. Biomed. Eng.* **5**, 737–748 (2021).
22. Luo, Y. F. et al. Technology roadmap for flexible sensors. *ACS Nano*. https://doi.org/10.1021/acsnano.2c12606 (2023).
23. Bandodkar, A. J., Jeang, W. J., Ghaffari, R. & Rogers, J. A. Wearable sensors for biochemical sweat analysis. *Annu. Rev. Anal. Chem.* **12**, 1–22 (2019).
24. Vinoth, R., Nakagawa, T., Mathiyarasu, J. & Mohan, A. M. V. Fully printed wearable microfluidic devices for high-throughput sweat sampling and multiplexed electrochemical analysis. *ACS Sens.* **6**, 1174–1186 (2021).
25. Hu, J., Stein, A. & Bühlmann, P. Rational design of all-solid-state ion-selective electrodes and reference electrodes. *Trac Trends Anal. Chem.* **76**, 102–114 (2016).
26. Shao, Y., Ying, Y. & Ping, J. Recent advances in solid-contact ion-selective electrodes: functional materials, transduction mechanisms, and development trends. *Chem. Soc. Rev.* **49**, 4405–4465 (2020).
27. Alizadeh, A. et al. A wearable patch for continuous monitoring of sweat electrolytes during exertion. *Lab Chip* **18**, 2632–2641 (2018).
28. Mou, L., Xia, Y. & Jiang, X. Epidermal sensor for potentiometric analysis of metabolite and electrolyte. *Anal. Chem.* **93**, 11525–11531 (2021).
29. Pirovano, P. et al. A wearable sensor for the detection of sodium and potassium in human sweat during exercise. *Talanta* **219**, 121145 (2020).
30. Hao, J. et al. Photosensitive-stamp-inspired scalable fabrication strategy of wearable sensing arrays for noninvasive real-time sweat analysis. *Anal. Chem.* **94**, 4547–4555 (2022).
31. Huang, X. et al. Garment embedded sweat-activated batteries in wearable electronics for continuous sweat monitoring. *npj Flex. Electron* **6**, 10 (2022).
32. Vázquez, M., Bobacka, J., Ivaska, A. & Lewenstam, A. Influence of oxygen and carbon dioxide on the electrochemical stability of poly(3,4-ethylenedioxythiophene) used as ion-to-electron transducer in all-solid-state ion-selective electrodes. *Sens. Actuators B Chem.* **82**, 7–13 (2002).
33. Yuan, D. et al. All-solid-state potentiometric sensors with a multiwalled carbon nanotube inner transducing layer for anion detection in environmental samples. *Ana. Chem.* **87**, 8640–8645 (2015).
34. Cheng, X. et al. A mediator-free electroenzymatic sensing methodology to mitigate ionic and electroactive interferents' effects for reliable wearable metabolite and nutrient monitoring. *Adv. Funct. Mater.* **30**, 1908507 (2020).
35. Li, M. et al. A highly integrated sensing paper for wearable electrochemical sweat analysis. *Biosens. Bioelectron.* **174**, 112828 (2021).
36. Shi, Z. et al. Wearable battery-free theranostic dental patch for wireless intraoral sensing and drug delivery. *npj Flex. Electron* **6**, 49 (2022).
37. Welch, E. C. et al. Advances in biosensors and diagnostic technologies using nanostructures and nanomaterials. *Adv. Funct. Mater.* **31**, 2104126 (2021).
38. Jaworska, E. et al. Gold nanoparticles solid contact for ion-selective electrodes of highly stable potential readings. *Talanta* **85**, 1986–1989 (2011).
39. Zhai, Q. et al. Vertically aligned gold nanowires as stretchable and wearable epidermal ion-selective electrode for noninvasive multiplexed sweat analysis. *Anal. Chem.* **92**, 4647–4655 (2020).
40. Wang, R. et al. Stretchable gold fiber-based wearable textile electrochemical biosensor for lactate monitoring in sweat. *Talanta* **222**, 121484 (2021).
41. Wang, S. et al. Wearable sweatband sensor platform based on gold nanodendrite array as efficient solid contact of ion-selective electrode. *Anal. Chem.* **89**, 10224–10231 (2017).
42. Xu, J. et al. Simple and efficient synthesis of gold nanoclusters and their performance as solid contact of ion selective electrode. *Electrochim. Acta* **222**, 1007–1012 (2016).
43. Zhao, Y. et al. A wearable freestanding electrochemical sensing system. *Sci. Adv.* **6**, eaaz0007 (2020).
44. Tavakoli, M. et al. 3R electronics: scalable fabrication of resilient, repairable, and recyclable soft-matter electronics. *Adv. Mater.* **34**, 2203266 (2022).
45. Tan, M. et al. Recent advances in intelligent wearable medical devices integrating biosensing and drug delivery. *Adv. Mater.* **34**, 2108491 (2022).
46. Wang, S. et al. Intrinsically stretchable electronics with ultrahigh deformability to monitor dynamically moving organs. *Sci. Adv.* **8**, eabl5511 (2022).
47. Xu, G. et al. Battery-free and wireless smart wound dressing for wound infection monitoring and electrically controlled on-demand drug delivery. *Adv. Funct. Mater.* **31**, 2100852 (2021).
48. Martinez, A. W., Phillips, S. T., Whitesides, G. M. & Carrilho, E. Diagnostics for the developing world: microfluidic paper-based analytical devices. *Anal. Chem.* **82**, 3–10 (2010).
49. Yang, M. P. et al. Paper-based sandwich-structured wearable sensor with sebum filtering for continuous detection of sweat pH. *ACS Sens* **8**, 176–186 (2023).
50. Noviana, E. et al. Electrochemical paper-based devices: sensing approaches and progress toward practical applications. *Lab Chip* **20**, 9–34 (2020).
51. Fang, H. et al. Simultaneously detecting monoamine oxidase A and B in disease cell/tissue samples using paper-based devices. *ACS Appl. Bio Mater.* **4**, 1395–1402 (2021).
52. Chiang, H. C., Wang, Y., Zhang, Q. & Levon, K. Optimization of the electrodeposition of gold nanoparticles for the application of highly sensitive, label-free biosensor. *Biosensors* **9**, 50 (2019).
53. Liu, A. et al. Fabrication and characterization of gold nanoclusters on phosphorus incorporated tetrahedral amorphous carbon electrode. *Electrochem. Commun.* **10**, 827–830 (2008).
54. Zahed, M. A. et al. A nanoporous carbon-MXene heterostructured nanocomposite-based epidermal patch for real-time biopotentials and sweat glucose monitoring. *Adv. Funct. Mater.* **32**, 2208344 (2022).
55. Laochai, T. et al. Non-invasive electrochemical immunosensor for sweat cortisol based on L-cys/AuNPs/ MXene modified thread electrode. *Biosens. Bioelectron.* **203**, 114039 (2022).
56. An, Q. et al. A multichannel electrochemical all-solid-state wearable potentiometric sensor for real-time sweat ion monitoring. *Electrochem. Commun.* **107**, 106553 (2019).
57. Baker, L. B. Physiology of sweat gland function: the roles of sweating and sweat composition in human health. *Temperature* **6**, 211–259 (2019).
58. Sonner, Z. et al. The microfluidics of the eccrine sweat gland, including biomarker partitioning, transport, and biosensing implications. *Biomicrofluidics* **9**, 031301 (2015).
59. Morgan, R. M., Patterson, M. J. & Nimmo, M. A. Acute effects of dehydration on sweat composition in men during prolonged exercise in the heat. *Acta Physiol. Scand.* **182**, 37–43 (2004).
60. Heitland, P. & Köster, H. D. Biomonitoring of 30 trace elements in urine of children and adults by ICP-MS. *Clin. Chim. Acta* **365**, 310–318 (2006).

ACKNOWLEDGEMENTS

This work was financially supported by the National Key R&D Program of China (2020YFA0709900, 2021YFB3200302), the National Natural Science Foundation of China (62288102, 22075139, 22077101), and Fundamental Research Funds for the Central Universities.

AUTHOR CONTRIBUTIONS

W.J. and H.L. are the co-first author. W.J.: conceptualization, data curation, formal analysis, writing—original draft, writing—review & editing. H.L.: conceptualization, data curation, formal analysis, writing – original draft, writing – review & editing. Y.L.: data curation, formal analysis, writing – review & editing. W.Z.: data curation, formal analysis, writing—review & editing. T.Z.: data curation, formal analysis, writing—review & editing. X.L., J.D., B.Z., R.X., A.D.: data curation, writing—review & editing. C.T.: writing—review & editing, supervision, project administration. J.W.: writing—review & editing, supervision, project administration. Q.W.: conceptualization, writing – review & editing, supervision, project administration. W.Z.: conceptualization, writing – review & editing, supervision, project administration. L.L.: conceptualization, writing – review & editing, supervision, project administration. F.H.: conceptualization, writing – review & editing, visualization, supervision, project administration.

COMPETING INTERESTS

The authors declare no competing interests.

ADDITIONAL INFORMATION

Supplementary information The online version contains supplementary material available at https://doi.org/10.1038/s41528-023-00285-w.

Correspondence and requests for materials should be addressed to Qiong Wu, Lin Li or Fengwei Huo.